JOURNAL OF MATERIALS SCIENCE 26 (1991) 341–348

Deformation and fracture of cork in tension

M. E. ROSA, M. A. FORTES
Departamento de Engenharia de Materiais, Instituto Superior Tecnico, Av. Rovisco Pais, 1000 Lisboa, Portugal

Various properties related to the deformation and fracture of cork in tension were experimentally determined, including the Young's modulus, the stress and strain at fracture and the fracture toughness K_{Ic}. The transverse isotropy of cork implies that there are three independent systems of mode I crack propagation and K_{Ic} was measured for each. The mechanisms of deformation and fracture were identified by SEM microscope observation of *in situ* deformation and of the fracture surfaces and crack paths. Two fundamental mechanisms of fracture occur: crack propagation along the lateral cell walls in non-radial tension, with $K_{Ic} = 94 \pm 16\ \text{kPa m}^{1/2}$ and crack propagation by breaking the cell walls in radial tension with $K_{Ic} = 125 \pm 14\ \text{kPa m}^{1/2}$. In radial tension, local fractures that do not propagate due to crack stopping were observed which lead to serrations in the tensile curves for that direction. The strain to fracture in this direction is considerably larger than in the perpendicular (non-radial) directions.

1. Introduction

In contrast to the relatively good characterization and understanding of the behaviour of cork under uniaxial [1, 2] and hydrostatic [3] compression, little is known about its tensile and fracture properties. Nevertheless, in its applications cork is frequently submitted to tensile stresses which sometimes lead to fracture (e.g. when a cork screw is introduced in a stopper, or when the stopper is removed from the bottle). Tangential tensile stresses due to growth also occur in cork while it is still in the tree, which may lead to axial cracks in the outer cork layers [4].

In this paper we report on an experimental study of the deformation and fracture behaviour of cork in tension aimed at the determination of various properties and at the identification of the relevant mechanisms.

In the first approximation cork is a transversally isotropic material, the radial direction (to be denoted by R) being a direction of symmetry of the cellular structure (Fig. 1). This is because the prismatic cells in cork are packed in columns parallel to the radial direction while the orientation of the lateral faces of the cells is essentially random. The non-radial directions (i.e. those perpendicular to the radial direction, including the axial (A) and tangential (T) directions) are then approximately equivalent. The symmetry of the radial direction is not destroyed by the lenticular channels which always occur in cork and run parallel to the radial direction [4]. The lateral cell walls are more or less corrugated, and this plays an important role in the compression properties [1, 2]. The cell bases have a staggered arrangement; they are in general not plane and slightly inclined in relation to the tangential plane.

In this study, tensile properties of cork were evaluated in uniaxial tensile tests of unnotched specimens, the direction of tension being, in different tests, parallel to each of the principal directions in cork (i.e., R, A and T directions).

Fracture tests were performed in notched specimens loaded in simple tension and in bending under conditions that lead to various systems of propagation of mode I cracks. A system of propagation is identified by the plane of the crack (indicated by the direction of its normal, which coincides with the direction of tension) and by the direction of propagation of the crack, in this order (Fig. 2). For example, in the system RA, the crack plane is perpendicular to the radial direction and propagates in the axial direction when stressed in the radial direction. In virtue of the symmetry of the structure of cork, only three independent systems of propagation are to be expected, namely RA = RT; AR = TR and AT = TA (Fig. 2). Nevertheless, the six systems were tested in order to confirm the equivalences predicted by symmetry.

For cracks propagating in the radial direction there may be differences between inward and outward propagation relative to the tree trunk, because of a different distribution of the internal growth stresses, but this was not investigated. A possible difference between upward and downward crack propagation in the axial direction was also not considered.

The tensile [6] and fracture [7] properties of various woods are fairly well characterized and K_{Ic} values have been measured for the various propagation systems. Since wood is orthotropic there are six propagation systems to be considered. The fracture toughness and the fracture stress are usually very anisotropic (e.g. a factor of $\simeq 12$ in the K_{Ic} values for pine wood [7]). Two main fracture mechanisms related to different crack paths were identified in wood [7]. In one, observed in the TA, TR, RA and RT systems, the crack propagates along the cell walls, with relatively low K_{Ic}

0022–2461/91 $03.00 + .12

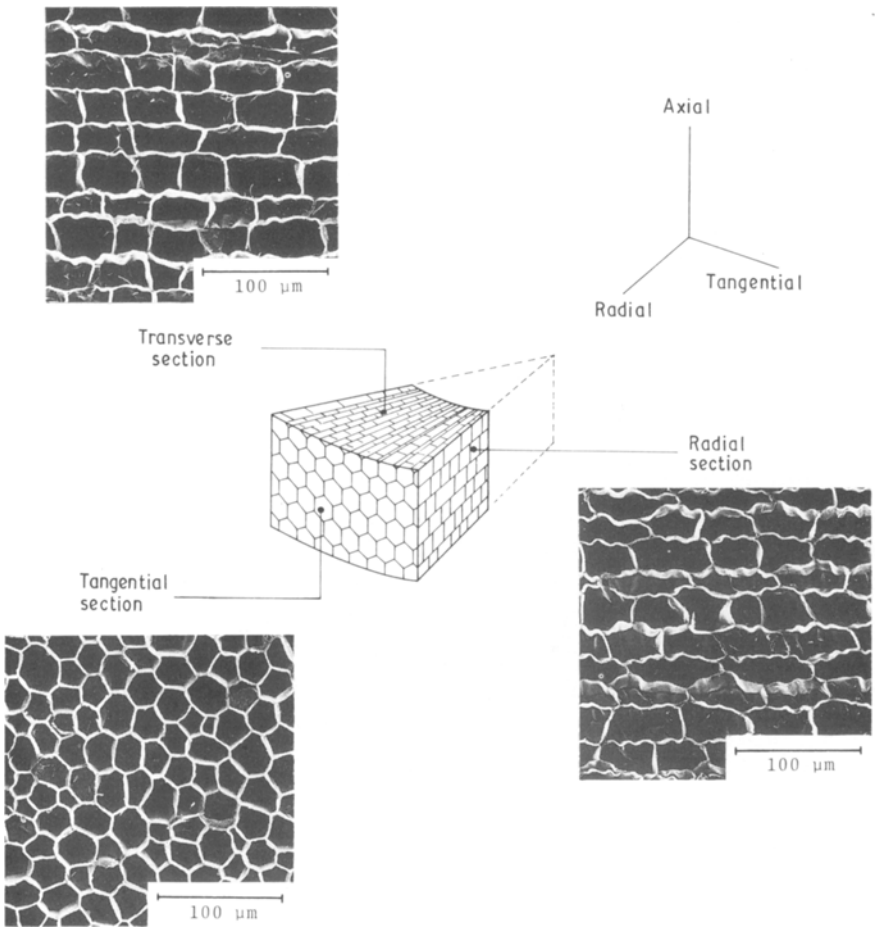

Figure 1 Schematic representation of the cellular structure of cork with indication of the principal directions. SEM images of sections perpendicular to those directions. Note that the transverse and radial sections have the same aspect, indicating the equivalence of non-radial directions.

values. In the other, with larger K_{Ic}, the crack propagates by breaking the cell walls transversally; this happens for the other propagation systems (AT and AR). As will be shown, the same two types of crack propagation are observed in cork.

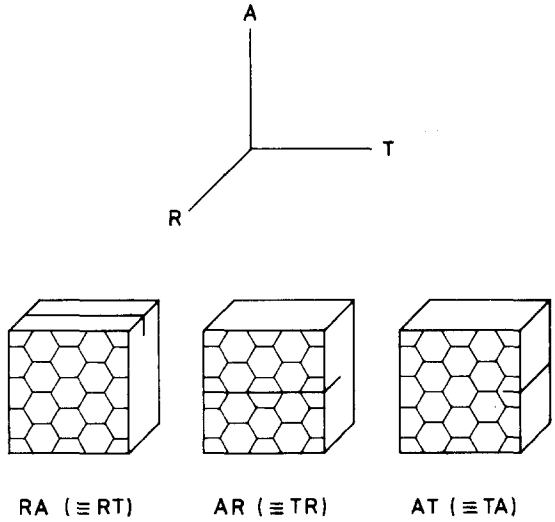

Figure 2 The three independent systems of crack propagation. The first letter indicates the normal to the plane of the crack which coincides with the direction of tension. The second letter indicates the direction in which the crack advances. R is the radial direction and NR a non-radial direction, such as the axial (A) and tangential (T) directions.

2. Experimental procedure

The cork used in the experiments was a reproduction cork of first industrial quality (low porosity) previously submitted to a boiling operation, which consists of immersion of the cork boards in boiling water for about 1 h [8]. Its density, upon equilibration with the laboratory atmosphere, was 154 kg m^{-3}, with a moisture content of 5%. Scanning electron microscope (SEM) images of the three principal sections are shown in Fig. 1.

The specimens for plain tensile tests were in the form of plates, 30 mm wide and 5 mm thick. The length of the specimens loaded in the non-radial directions (axial and tangential) was 60 mm, while those loaded in the radial direction were limited to a length of $\sim$ 20 mm by the thickness of the cork board. The specimens were gripped to the machine at their extremities with an intermediate 1 mm sheet of aluminium in the way shown in Fig. 3.

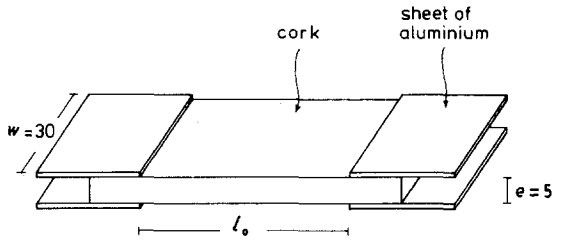

Figure 3 Unnotched specimens used in tensile tests. The dimensions are indicated in mm.

TABLE 1 Properties of cork measured in plain tension tests at $\dot{\epsilon} = 8.3 \times 10^{-4}\,sec^{-1}$.

Tensile direction	E (MPa)	Serrations				σ_f (MPa)	ϵ_f (%)
		$\sigma_{beginning}$ (MPa)	$\epsilon_{beginning}$ (%)	σ_{end} (MPa)	ϵ_{end} (%)		
Radial	38.1 ± 7.0	0.36 ± 0.14	1.23 ± 0.58	0.49 ± 0.20	7.91 ± 6.40	1.15 ± 0.10	18.0 ± 11.2
Axial	24.2 ± 4.1	—	—	—	—	0.70 ± 0.16	7.7 ± 2.2
Tangential	26.0 ± 4.4	—	—	—	—	0.82 ± 0.18	7.5 ± 2.7

Most tensile tests were undertaken at a strain rate of $8.3 \times 10^{-4}\,sec^{-1}$. Three specimens were tested for each of the non-radial directions and six for the radial direction of tension. Further tests were conducted at a strain rate of $8.3 \times 10^{-5}\,sec^{-1}$ in non-radial directions in order to study rate effects.

Small specimens were observed in the SEM in a device that allowed *in situ* tensile loading. A surface parallel to the direction of loading was observed at successive stages during incremental straining.

Two types of notched specimens were used in the tests aimed at characterizing the mode I fracture behaviour of cork: double-notched tensile specimens (used for all propagation systems) and notched three-point bending specimens (used only for cracks lying in planes perpendicular to non-radial directions, because of limitations in size). The double-notched specimens (Fig. 4a) had the same dimensions as the plain tension specimens, with two notches of depth c symmetrically placed in the specimens. The dimensions of the three-point bending specimens are indicated in Fig. 4b.

Two values, 5 and 10 mm, of the notch depth, c, were used in both types of specimens. The notches were produced by a sharp steel blade to the required depth, which was then accurately measured with a micrometer eye-piece. The strain rate in the double-notched tensile tests was $8.3 \times 10^{-4}\,sec^{-1}$. The bending tests were performed at a cross-head speed of $3\,mm\,min^{-1}$.

The fracture surface of the notched specimens was observed by SEM. Razor-blade sections perpendicular to the fronts of cracks that had not completely propagated to cause rupture were also observed by SEM. All SEM specimens were coated with a ~ 20 nm layer of gold prior to observation.

3. Results and discussion

3.1. Mechanical tests

Average stress–strain curves obtained in tensile tests of plain specimens at a strain rate of $83 \times 10^{-4}\,sec^{-1}$ are shown in Fig. 5. The curves for the two non-radial directions (A and T) are nearly coincident, although the tangential direction was consistently found to be slightly more resistant than the axial direction. The same small difference in strength between these two directions is also observed in uniaxial compression [2]. The curve for the radial direction (R) is quite different and shows an intermediate region with serrations. Very few or no serrations were observed in the non-radial curves. Relevant average quantities that can be drawn from the stress-strain curves are indicated in Table I. Since the initial part of the curve is not linear, the Young's modulus was calculated from the average slope between 0.1 and 0.2% strain. Also indicated in Table I are the stress and strain at fracture and the stress and strain intervals over which serrations were observed in the radial tension curves. The radial direction is more stiff and shows a larger fracture stress, although at intermediate strains its

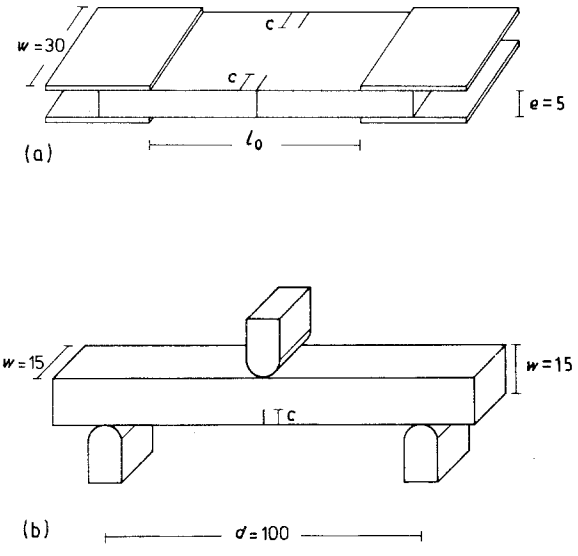

Figure 4 Notched specimens: (a) tensile tests; (b) three-point bending tests. The dimensions are indicated in mm.

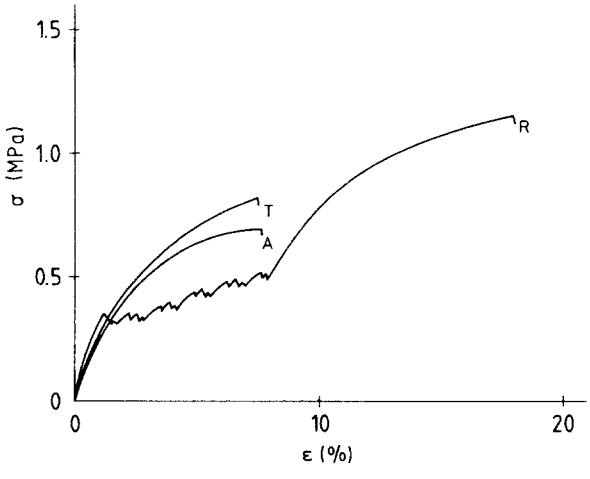

Figure 5 Stress–strain curves in tensile tests of unnotched specimens loaded in each of the three principal directions, with $\dot{\epsilon} = 8.3 \times 10^{-4}\,sec^{-1}$.

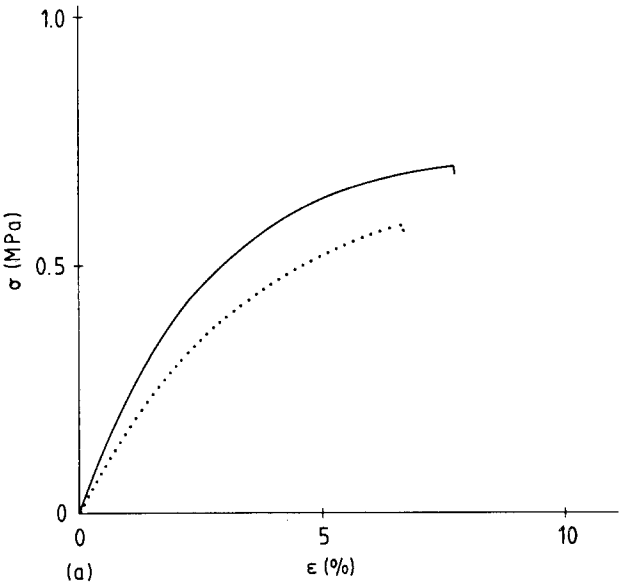

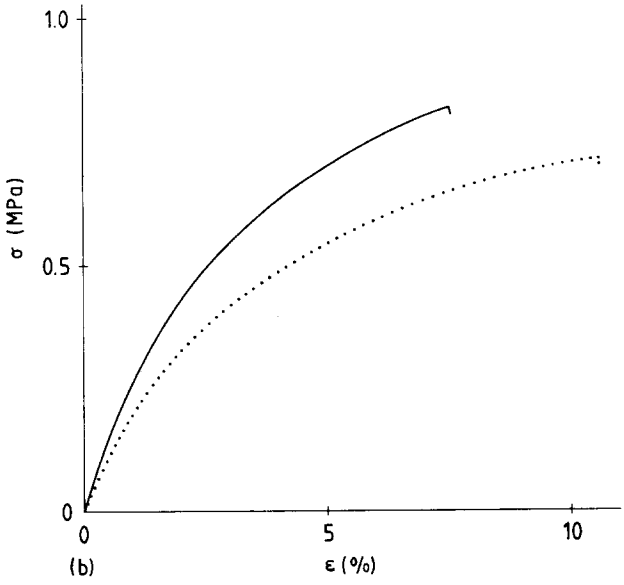

Figure 6 Effect of strain rate on the stress–strain curve in the non-radial directions: (a) axial; (b) tangential. Full line: $\dot{\varepsilon} = 8.3 \times 10^{-4}\ \text{sec}^{-1}$; dotted line; $\dot{\varepsilon} = 8.3 \times 10^{-5}\ \text{sec}^{-1}$.

strength is below that for the non-radial directions. The strain at fracture is considerably larger in the radial direction.

Young's moduli in compression were measured in other specimens of the same cork at the same strain rates and found to be appreciably smaller [cf. ref. 2], by as much as a factor of 3.

The effect of strain rate on the stress-strain curve in non-radial tension is shown in Fig. 6. A strain rate sensitivity $m = d\,\ell n\,\sigma / d\,\ell n\,\dot{\varepsilon}$ can be calculated from these curves, with a value near 0.1, fairly independent of strain. This value of m is comparable to the one that can be obtained in compression [2]. The Young's modulus decreases as the strain rate decreases, the value for $\dot{\varepsilon} = 8.3 \times 10^{-5}\ \text{sec}^{-1}$ being 19.0 MPa compared with 25 MPa for $\dot{\varepsilon} = 8.3 \times 10^{-4}\ \text{sec}^{-1}$ (see Table I). No systematic effect of the strain rate on the stress and strain at fracture in non-radial directions was observed.

Stress–strain curves of double-notched tensile specimens are shown in Fig. 7 for 10 mm deep notches for

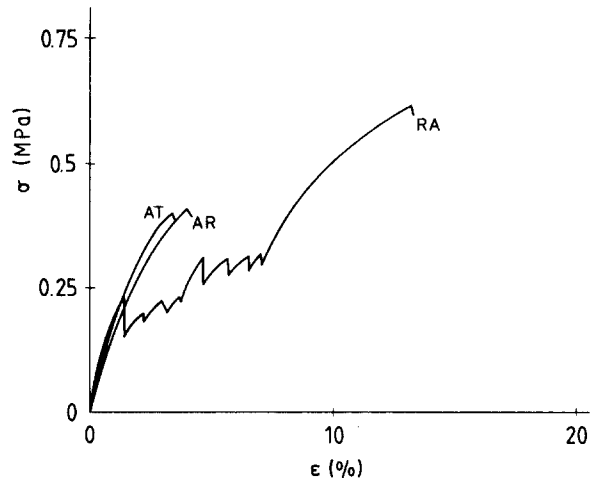

Figure 7 Stress–strain curves in tensile tests of double-notched specimens (notch depth of 10 mm) for three crack propagation systems.

three systems of crack propagation. The stress is load divided by initial area of cross section in the notched region. The curves for other equivalent systems of crack propagation are very close to the corresponding curves of Fig. 7. The curves for the notched specimens are similar to those shown in Fig. 5 for plain specimens, but, as expected, the stress and strain at fracture are smaller than in the plain specimens, decreasing as the notch depth increases. The serrated region in radial tension is still observed in the notched specimens. Fracture occurs at the maximum, final, load.

Load–deflection curves obtained in the three-point bending tests of notched specimens are shown in Fig. 8 for the two notch depths used. Catastrophic fracture occurs at the maximum load.

Values of the fracture toughness, K_{Ic}, were calculated from the equations of linear elastic fracture mechanics, as was done for wood by Ashby *et al.* [7]. For the double-notched tensile specimens

$$K_{Ic} = \frac{2F_f}{ew}(\pi c^{1/2}) f_1\,(c/w) \qquad (1)$$

and for the three-point bending specimens

$$K_{Ic} = \frac{F_f d}{ew^{3/2}} f_2(c/w) \qquad (2)$$

F_f is the load at fracture, f_1 and f_2 are geometrical factors that depend on c/w [9], and the other quantities are indicated in Figs 3 and 4.

Values of K_{Ic} calculated from Equations 1 and 2, respectively, can be found in Tables II and III. The dispersion of values is quite large, but some general trends can be noted. Firstly, the values of K_{Ic} are nearly the same for the equivalent systems of propagation, i.e. RA = RT, AR = TR and AT = TA. It is then convenient to designate the non-radial directions by NR and the three independent systems by R–NR, NR–R and NR–NR. The K_{Ic} values are fairly independent of the notch depth but a tendency is observed for larger values of K_{Ic} in the tensile tests relative to the bending tests. Finally, it is apparent that the K_{Ic} values for the systems NR–R and NR–NR are very similar, but appreciably smaller than those for the

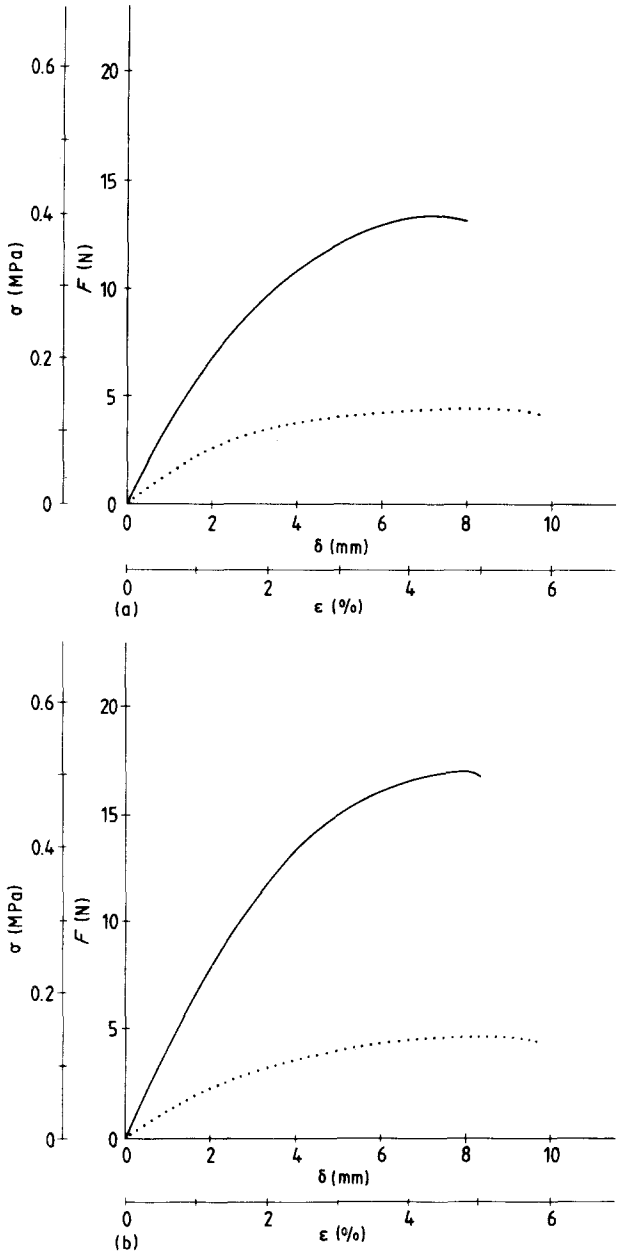

Figure 8 Load (F)–deflection (δ) curves in three-point bending notched specimens for two crack propagation systems: (a) AR; (b) AT. Full line: notch depth, 5 mm; dotted line: notch depth, 10 mm. The tensile stress and strain at the more stressed regions are given in the σ and ϵ scales, respectively.

TABLE II K_{Ic} values determined from double notch tension tests.

System of propagation	Notch depth	K_{Ic} (kPa $m^{1/2}$)
RA	5	125.5 ± 5.7
	10	127.6 ± 12.6
RT	5	127.8 ± 18.5
	10	116.8 ± 28.0
AR	5	91.8 ± 7.6
	10	95.5 ± 7.1
TR	5	90.9 ± 25.5
	10	103.0 ± 28.0
AT	5	80.1 ± 5.0
	10	91.3 ± 4.1
TA	5	96.1 ± 24.1
	10	103.2 ± 9.9

TABLE III K_{Ic} values determined from three point bending tests of notched specimens.

System of propagation	Notch depth	K_{Ic} (kPa $m^{1/2}$)
AR	5	70.8 ± 1.1
	10	67.8 ± 0.5
TR	5	91.0 ± 19.1
	10	59.6 ± 12.4
AT	5	91.8 ± 0.1
	10	62.4 ± 1.4
TA	5	63.5 ± 0.3
	10	61.4 ± 5.8

R–NR system. The reason for this may be related to the mechanism of fracture in the different systems, to be discussed below.

3.2. Scanning electron microscope observations

The fracture surfaces observed in SEM are shown in Fig. 9 for each system of propagation. SEM images of the cross-sections of cracks propagating in each system can be seen in Fig. 10. From these observations,

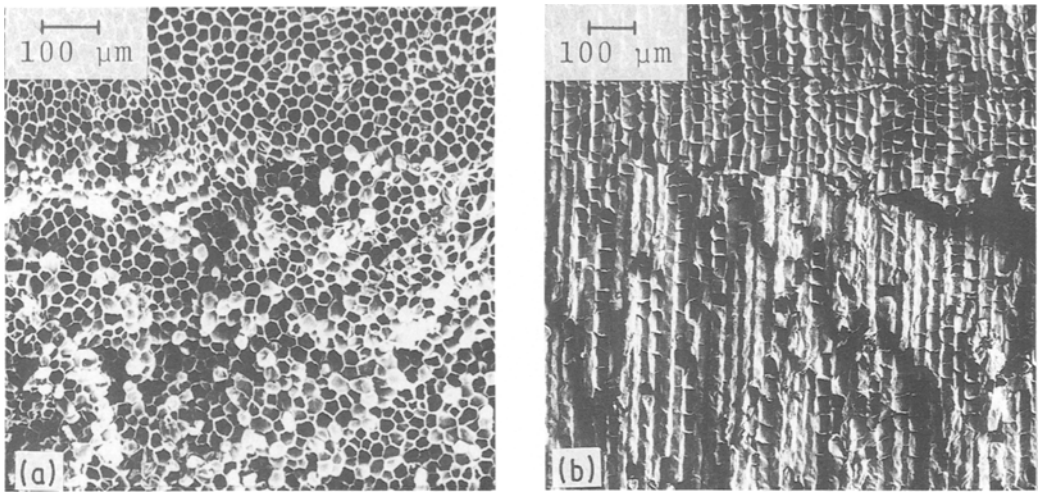

Figure 9 Fracture surfaces observed in the SEM after crack propagation in the following systems: (a) R–NR; (b) NR–R. The fracture surface for the system NR–NR is similar to that for the system NR–R. On the top of the photographs the end of the surface of the notch can be seen.

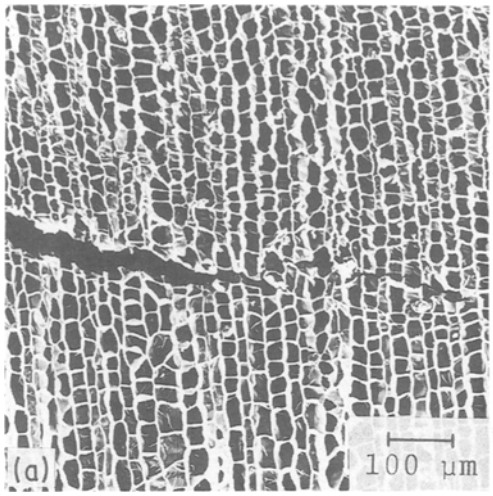

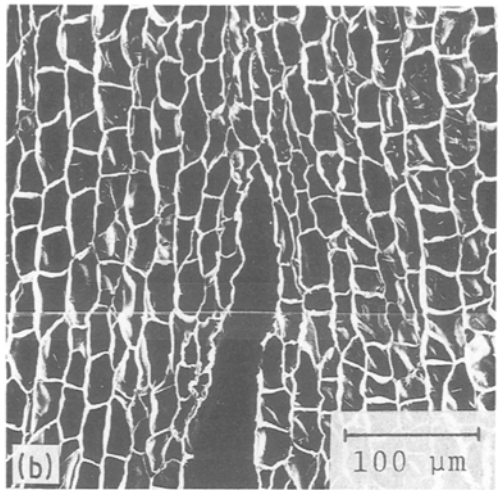

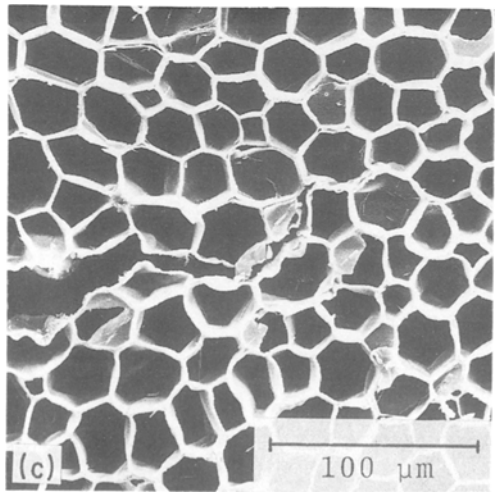

Figure 10 Cross-sections through the crack front in the following propagation systems: (a) R–NR; (b) NR–R; (c) NR–NR.

the crack path in each case can be inferred. When the plane of the crack is perpendicular to the radial direction (R–NR system), the crack advances by breaking the lateral cell walls as shown schematically in Fig. 11a. The number of cell bases at the surface level of the specimen is then relatively small (Fig. 9a) while broken lateral walls can be identified in the cross-section. In the other systems (NR–R and NR–NR), for which the plane of the crack is parallel to the radial direction, the crack advances along the lateral cell walls, splitting them longitudinally, as shown schematically in Fig. 11b, c. Evidence for this can be seen in Fig. 9b where the number of cell walls at the surface level is larger than in a random cut through cork and also in Fig. 10b and c where broken walls can be seen. The fact that the same mechanism of fracture operates in the NR–R and NR–NR systems may explain the similarity of K_{Ic} and fracture stress values measured for the two systems.

The *in situ* observations show that as cork is stressed in tension the cell walls are stretched. The lateral walls in radial tension become more straight, i.e. the amplitude of the undulations progressively decreases and the lateral walls tend to orientate themselves parallel to the direction of tension. Similar effects are observed in the cell bases in NR tension. Also interesting is the observation made in radial tension of localized fracture of the lateral walls of a cell which propagates to a few surrounding cells and then stops. These localized fracture events occur at low strains and are probably related to the serrations observed in the stress–strain curves in radial tension. When a local fracture occurs at a weak or over-stressed wall, an increment of strain results and therefore the stress decreases, because of the imposed constant strain rate. The fact that these fractures do not lead to global fracture indicates that the associated crack stops. The *in situ* SEM observations show that there is some blunting of the crack due to the straightening of the adjacent lateral walls. Furthermore, the crack front may be stopped by the cell edges which are presumably obstacles to crack propagation. The end of the serrated region in the stress–strain curve could then be associated with an exhaustion of the weak regions that give localized fractures. It is difficult, however, to understand how the stress can still rise to much larger values (the global fracture stress) without giving rise to more localized fractures.

When the direction of tension is non-radial, there is no indication of localized fracture events of the type observed in radial tension. Fracture only occurs at the maximum, final load.

4. Summary

A fairly clear picture of the deformation and fracture of cork under tension emerges from this study. When tension is applied to cork, the cell walls become straighter and aligned in the direction of tension. Further deformation occurs by stretching of the walls. There is a marked effect in strain rate, indicating an important viscous component of deformation. The larger Young's moduli observed in tension compared to compression can be explained in terms of the stiffness of undulated plates (the cell walls), which increases as the amplitude of the undulations decreases. While compression increases the amplitude, tension decreases it.

In radial tension there are incipient localized fracture events which give rise to serrations in the tensile

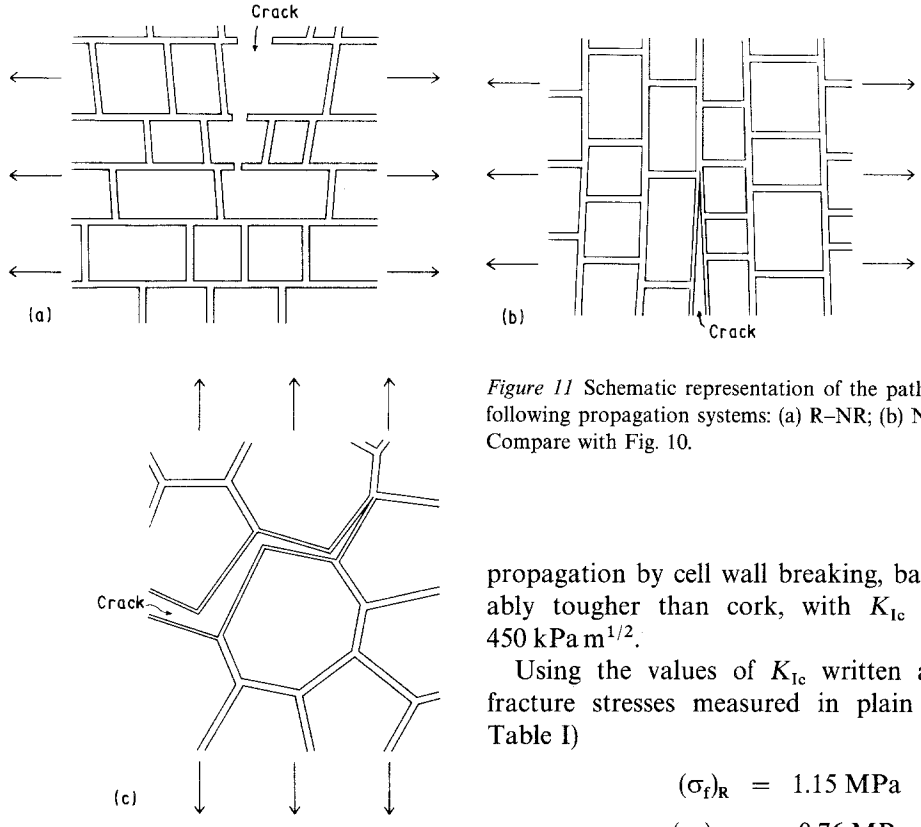

Figure 11 Schematic representation of the path of a crack in the following propagation systems: (a) R–NR; (b) NR–R; (c) NR–NR. Compare with Fig. 10.

curve. The reason why these serrations stop at relatively low stresses, well before global fracture, is uncertain.

Two different mechanisms of mode I fracture were identified. In one, that occurs when cork is stressed in the radial direction, fracture occurs by transverse breaking of the lateral cell walls. In the other, that occurs when cork is stressed in a non-radial direction, fracture occurs along the walls, which are longitudinally split into two half-walls. The cell walls are known to be formed by various layers or lamellae symmetrically placed on each side of a middle lamella [4]. This type of fracture probably occurs by separation along the interface between two weakly bound lamellae. There is a continuous path for a running crack along the lateral cell walls, because the cells are disposed in columns, in spite of the fact that the crack root is necessarily segmented since the successive walls where it is located are not coplanar. A similar continuous path is not available for a crack running along the cell bases; the fracture mode in NR tension is then replaced by the transverse breaking of the lateral walls.

The K_{Ic} values obtained for the two fracture mechanisms show a very large scatter, but the following average values (taken from double-notch tension tests) can be indicated

$$(K_{Ic})_R = 125 \pm 14\,\text{kPa}\,\text{m}^{1/2}$$

$$(K_{Ic})_{NR} = 94 \pm 16\,\text{kPa}\,\text{m}^{1/2}$$

These values for cork can be compared with those for balsa [7], a wood with a density similar to that of cork. The K_{Ic} values for crack propagation along the cell walls are comparable in the two materials, but for propagation by cell wall breaking, balsa is considerably tougher than cork, with K_{Ic} values around 450 kPa $m^{1/2}$.

Using the values of K_{Ic} written above and the fracture stresses measured in plain specimens (cf. Table I)

$$(\sigma_f)_R = 1.15\,\text{MPa}$$

$$(\sigma_f)_{NR} = 0.76\,\text{MPa}$$

it is possible to calculate, from Equation 1, the size of the "intrinsic" defect responsible for fracture. The values are

$$c_R = 4(\pm 2)\,\text{mm}$$

$$c_{NR} = 6(\pm 4)\,\text{mm}$$

comparable to the smallest notch depth used in the fracture tests. Nevertheless, fracture always started at the root of the notches. In NR-tension the pores act as stress concentrators and the intrinsic defect is probably a pore, presumably located at the surface, in agreement with the c_{NR} value of (6 ± 4) mm. There is experimental evidence that the cross-section of the pores is approximately elliptical, with the longer axis in the tangential direction. This could explain the small difference in strength between the axial and tangential directions, since a larger stress concentration is to be expected when the pore is stressed in the direction of its shorter diameter. In R-tension, the effect of pores as stress concentrators is negligable (they only reduce the effective area of the cross-section) and the intrinsic defect cannot be identified with a pore. The *in situ* SEM observations suggest that in R-tension, the critical defect is not present *ab initio*, but results from the coalescence of several localized fractures.

Acknowledgement

This work was financially supported by the Instituto de Ciência e Tecnologia dos Materials, Lisboa.

References

1. L. J. GIBSON, K. E. EASTERLING and M. F. ASHBY, *Proc. R. Soc.* **A377** (1981) 99–117.

2. M. EMÍLIA ROSA and M. A. FORTES, *J. Mater. Sci.* **23** (1988) 879–885.
3. M. A. FORTES, J. J. FERNANDES, I. SERRALHEIRO and M. E. ROSA, *J. Testing Evaluation* **17**, (1989) 67–71.
4. J. VIEIRA NATIVIDADE. "Subericultura", Ministério da Economia, Direcção dos Serviços Florestais e Aquícolas, Lisboa, 1950.
5. HELENA PEREIRA, M. EMÍLIA ROSA and M. A. FORTES, *IAWA Bull.* **8** (1988) 213–218.
6. J. M. DINWOODIE "Timber its nature and behaviour" (Van Nostrand Reinhold, London, 1981).
7. M. F. ASHBY, K. E. EASTERLING, R. HARRYSSON and S. K. MAITI, *Proc. R. Soc.* **A398** (1985) 261–280.
8. M. EMÍLIA ROSA, HELENA PEREIRA and M. A. FORTES, *Wood Fiber Sci.* **22** (1990) 149–164.
9. D. P. ROOKE and D. J. CARTWRIGHT. "Compendium of stress intensity factors", Her Majesty's Stationery Office, London, 1976).

Received 16 October 1989
and accepted 20 March 1990